"Human displacements from tropical cyclone Idai attributable to climate change"

Benedikt Mester [1] [2], Thomas Vogt [1], Seth Bryant [2] [3], Christian Otto [1], Katja Frieler [1], and Jacob Schewe [1]

[1] Potsdam Institute for Climate Impact Research, Potsdam, Germany
[2] Institute of Environmental Science and Geography, University of Potsdam, Potsdam, Germany
[3] GFZ German Research Centre for Geosciences, Potsdam, Germany

Correspondence: Benedikt Mester (benedikt.mester@pik-potsdam.de)

Abstract

Extreme weather events, such as tropical cyclones, often trigger population displacement. The frequency and intensity of tropical cyclones is affected by anthropogenic climate change. However, the effect of historical climate change on displacement risk has so far not been quantified. Here, we show how displacement can be partially attributed to climate change, using the example of the 2019 tropical cyclone Idai in Mozambique. We estimate the population exposed to high water levels following Idai's landfall, using a combination of a 2D hydrodynamical storm surge model and a flood depth estimation algorithm to determine inland flood depths from remote sensing images, for factual (climate change) and counterfactual (no climate change) mean sea level and maximum wind speed conditions. Our main estimates indicate that climate change has increased displacement risk from this event by approximately 12,600 - 14,900 additional displaced persons, corresponding to about 2.7 to 3.2% of the observed displacements. The isolated effect of wind speed intensification is double that of sea level rise. These results are subject to important uncertainties related to both data and modeling assumptions, and we perform multiple sensitivity experiments to assess the range of uncertainty where possible. Besides highlighting the significant effects on humanitarian conditions already imparted by climate change, our study provides a blueprint for event-based displacement attribution.

1 Introduction

Between 1980 and 2021, an average of 45 tropical cyclones (TCs) globally have been recorded per year (Guha-Sapir et al., 2022). TCs pose a set of societal risks to coastal communities around the world. While related monetary losses are high, with an average of US$ 57.2 billion every year since 2008 (Guha-Sapir et al., 2022), TCs also displace an average of 9.3 million people every year, with this hazard being responsible for 43% of all weather-related displacements (IDMC, 2022). Such forced displacements are associated with human suffering, as well as substantial financial costs (e.g., for providing shelter or from loss

41 of economic production) and often require international assistance for disaster relief funds and
42 humanitarian response (Desai et al., 2021).
43
44 At the same time, global climate change is expected to alter TC characteristics, resulting in an
45 increase in overall TC intensity (maximum wind speed and precipitation) and hence in the
46 frequency of very intense TCs (category 4-5 on the Saffir-Simpson scale) (Knutson et al.,
47 2020). Primarily, this is the result of an increase in potential intensity due to warmer sea
48 surface temperatures (SST) (Emanuel, 2005, 2013, 1987). Sea level rise (SLR), also driven
49 by global warming, additionally compound coastal flood risk associated with TCs (e.g., Garner
50 Andra J. et al., 2017; Lin et al., 2012; Resio and Irish, 2016). Historic TC data records are
51 short and partially inconsistent, making it difficult to determine the degree of intensification
52 over time, despite observed changes in some basins, such as the South Indian Ocean
53 (Knutson et al., 2019; Kossin et al., 2013, 2007; Webster et al., 2005). Moreover, existing TC
54 datasets often focus on maximum wind speed, neglecting coastal and inland flooding which
55 may be the dominant hazards, e.g., as for Hurricane Katrina or Hurricane Harvey
56 (Bloemendaal et al., 2021). Paleo climate records (Lin et al., 2014; Nott and Hayne, 2001) and
57 synthetic TC tracks (Bloemendaal et al., 2022, 2020; Emanuel et al., 2006) can be used to
58 extend TC records.However, sediment availability is limited to a few coastal stretches and the
59 statistical resampling process incorporates only the average observed climatic conditions,
60 respectively, hampering the assessment of global climate change impacts over longer time
61 periods (Bloemendaal et al., 2020). Nonetheless, given that global mean surface air
62 temperature and sea level have already risen above pre-industrial conditions by about 1.1°C
63 and 0.20 m, respectively (Gulev et al., 2021), it is likely that recent TC landfalls have caused
64 more severe societal impacts than would be expected without climate change. A probabilistic
65 attribution addressing this topic is limited by the shortness of TC records (Trenberth et al.,
66 2015), and may be additionally affected by multi-decadal variability (e.g., the Atlantic
67 Multidecadal Oscillation) or interannual climate variability (e.g., the El Niño–Southern
68 Oscillation) (Patricola and Wehner, 2018). As a consequence, the portion of TC-induced
69 human displacements attributable to climate change has so far not been quantified.
70
71 In this study, we address this research gap for the particular case of displacement triggered
72 by TC Idai in 2019. We examine the floods in central Mozambique associated with TC Idai,
73 considered to be "one of the Southern Hemisphere's most devastating storms on record"
74 (Warren, 2019). On the 14th of March, Idai made landfall near the densely populated port city
75 of Beira, inhabited by more than 530,000 people (Figure 1). Alongside strong winds (maximum
76 1-min sustained winds of 180 km/h) and extensive inland flooding caused by heavy rainfall,
77 the cyclone also created a storm surge of up to 4.4 m, leading to coastal flooding centered at
78 the port city of Beira (Probst and Annunziato, 2019). In Mozambique alone, TC Idai claimed
79 the lives of more than 600 people, and caused 478,000 internal displacements, as well as
80 widespread structural damage totaling more than US$ 2.1 billion (Guha-Sapir et al., 2022;
81 IDMC, 2022).
82
83 Here, we investigate how the coastal flooding would have manifested in a counterfactual world
84 without climate change, and consequently, how many of the observed human displacements
85 from TC Idai can be linked to climate change. For the attribution of the impacts we follow the
86 storyline approach introduced by Shepherd (Shepherd, 2016). To this end, we account for two
87 known mechanisms through which global climate change could have affected coastal flood
88 hazard: SLR and amplification of storm intensity. Storm track and size are not changed, even

89 though both parameters are subject to the effects of climate change (Knutson et al., 2020,
90 2019). We first estimate the influence of climate change on sea level and TC intensity in the
91 South Indian Ocean. We employ a high-resolution hydrodynamic flood model to simulate TC
92 Idai's peak coastal flood extent and depth, both under historical conditions and under
93 counterfactual conditions with lower sea levels and lower maximum wind speed,
94 corresponding to a world without climate change. We additionally use satellite imagery to
95 account for inland (fluvial and pluvial) flooding, and estimate the total number of people
96 affected by flooding. We then model the number of displacements based on flood depth-
97 specific vulnerability factors, and estimate the fraction of displacements that can be attributed
98 to climate change by comparing results under factual vs. counterfactual conditions.
99
100 We use an estimate of SLR that attempts to separate natural variability in ice sheet and glacier
101 mass balance and retain only the long-term trend induced by global warming (Strauss et al.,
102 2021). Beyond this, however, our analysis is indifferent to whether the trends in sea level and
103 TC intensity are anthropogenic or not. This is in line with the definition of *impact attribution* put
104 forward by the Intergovernmental Panel on Climate Change (IPCC), where "changes in
105 natural, human, or managed systems are attributed to [a] change in [a] climate-related system"
106 (O'Neill et al., 2022). Such a question can be separated from the *climate attribution* question
107 of whether the change in the climate-related system - here, sea level and TCs - is due to
108 anthropogenic forcing. This separation allows us to focus on the link between climate change
109 and displacement despite remaining uncertainty about the exact anthropogenic contribution.
110 We will return to this issue in the discussion.
111
112 This study aims to attribute coastal-flood induced human displacements from TC Idai to
113 historic climate change, using a quantitative modeling approach. It addresses the need for
114 insights on the human impacts of climate change globally, and in particular in countries like
115 Mozambique that suffer from a combination of high exposure to climate-related hazards - in
116 this case, TCs - and high socio-economic vulnerability. Moreover, Mozambique, like many
117 other countries, is characterized by limited availability of in-situ observational data and a lack
118 of calibrated, local-scale inundation models. We use remote-sensing data and a globally
119 applicable modeling framework to characterize flood exposure during TC Idai; reported
120 displacement data is retrieved from the Global Internal Displacement Database (GIDD). Our
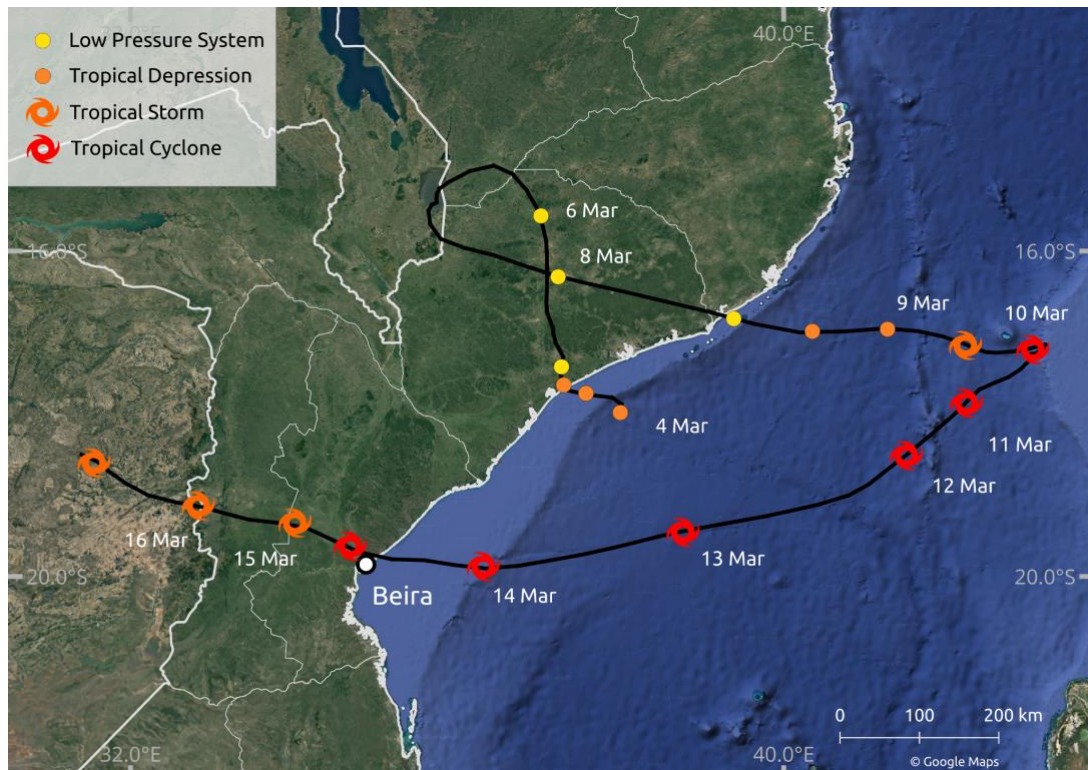121 approach is thus transferable to other cases in virtually all relevant countries.
122
123
124
125
126
127
128

Figure 1: Trajectory of tropical cyclone Idai over the South Indian Ocean. Trajectory data is based on the IBTrACS database (Knapp et al., 2010). Mozambican administrative boundaries (GADM, 2018) in white; satellite image background by © Google Maps (Google Maps (a), 2022). Dates and tropical cyclone status adopted from ReliefWeb (ReliefWeb, 2019a).

2 Methods

2.1 Counterfactuals

Constructing counterfactuals for sea level and TC intensity requires estimating the effect of historical climate change on these quantities. Total global mean sea level has risen by approximately 230 mm since the turn of the 20th century (Church and White, 2011); at a rate that has increased over time (Dangendorf Sönke et al., 2017). According to the IPCC, it is very likely that the rate of global mean SLR was 1.5 (1.1 to 1.9) mm yr^{-1} between 1902 and 2010, and 3.6 (3.1 to 4.1) mm yr^{-1} between 2006 and 2015 (Gulev et al., 2021). Nonetheless, regional changes in sea level may differ substantially from the global average due to shifting surface winds, the differential expansion of warming ocean water, and the addition of melting ice, which can alter the ocean circulation (Fox-Kemper et al., 2021). Additionally, increases in the amount of water stored on land (due to construction of dams and reservoirs), as well as land subsidence, have also affected total sea level, with their relative effects varying geographically (Church et al., 2004; Strauss et al., 2021).

Long-term in-situ observational records of SLR are scarce in the Indian Ocean (Han et al., 2010), hampering a precise detection of changes in sea level. For example, no active tide

gauge stations can be found on the coast of Beira (Beal et al., 2019), with the nearest station located in Inhambane, Mozambique, 448 km south of Beira. However, regional historical SLR rates for Mozambique, derived from satellite imagery or models, are close to global mean estimates. IPCC rates of change in sea surface height (geocentric sea level) derived from satellite altimetry show regional SLR off the coast of Mozambique at around 4.0 mm yr^{-1} for the period 1993–2012 (Church et al., 2013). Climate-induced SLR at the South-Eastern African coastline (1993 - 2015) is estimated at ~3.5 mm yr^{-1} using a coastal-length weighted approach (Nicholls et al., 2021). Reconstructed sea level fields using global tide gauge data suggests global-averaged SLR at 1.8 ± 0.3 mm yr^{-1} over the 1950-2000 period, with regional SLR off the coast of Mozambique at around 1.5 mm yr^{-1} (Church et al., 2004). Han and colleagues (Han et al., 2010) estimate regional Mozambican SLR at approximately 1.2 mm yr^{-1} between 1961-2008.

Given that these regional estimates are close to the global mean estimate by the IPCC, we assume that total SLR near Beira is the same as the global mean, a comparable approach as by Irish and colleagues (Irish et al., 2014). In order to exclude trends induced by natural variability, particularly in sea level contributions from glaciers and ice sheets, we use estimates of global mean sea level rise attributable to anthropogenic climate change for 1900–2012 from Strauss and colleagues (Strauss et al., 2021). Their ensemble estimate is 6.6 to 17.1 cm, which we use to define counterfactual sea level parameters for the coastal flood model. This also implies assuming no substantial local effects of land subsidence and human-induced changes in land water storage through reservoir construction and groundwater extraction that would confound comparison with the global estimates. This is hard to verify, but can be motivated by findings that city subsidence occurs only in a small fraction of the world's coasts (Nicholls et al., 2021).

Tropical cyclones are projected to become more intense with rising temperatures (Knutson et al., 2015), which is in line with the theoretical understanding of the potential intensity theory (Emanuel, 1987). Observed TC wind speed data in the South Indian Ocean basin shows that the maximum 10-minute sustained wind speed has been increasing by about 0.3 kn (0.15 m s^{-1}) per year on average, over the period 1973-2019 (Figure 2). Prior to 1973, the rate of increase was likely smaller, though observational data is lacking. We make a conservative assumption corresponding to 50 years of increase at a rate of 0.2 kn (0.1 m s^{-1}) per year, resulting in a total difference in maximum wind speed of approximately 10 kn (5.1 m s^{-1}). For the case of TC Idai with maximum observed 10-minute sustained wind speeds of 105 kn (54 m s^{-1}), this corresponds to a 10% reduction in maximum wind speed by removing climate change, which we adopt as a plausible assumption for counterfactual TC intensity.

This value is in line with the remote sensing-based estimates provided in Kossin et al. (2013), who find that lifetime maximum TC intensities in the SIO have increased by about 4.6 m/s over the period 1982-2009 (1.7 m/s per decade), which corresponds to 8.5% of TC Idai's maximum intensity. If this rate of increase is linearly extrapolated to 2019, it results in an increase of about 6.3 m/s (11.6%). Since the rate of increase has likely risen along with surface warming, and since our period of reference extends back to 1973 rather than 1982, a value of 12% might be a safer assumption for comparing the results of Kossin et al. (2013) with our own estimate. To quantify the effect of uncertainty in the estimate of TC intensity change, we conduct two sensitivity experiments, with counterfactual intensity lower than factual by 8.5% and 12%,

respectively, reflecting the SOI estimate of Kossin et al (2013) both directly and when extrapolated for comparability with our own estimate.

We note that lower rates of change have been found in climate model-based studies. Knutson et al. (2020) find a 6% increase in maximum intensity of SIO TCs per 2°C global mean surface warming. When applied to the historical increase in global mean surface temperatures of 1.1°C, this would yield an increase of 3.3%. While these climate model estimates are important both for assessing future changes and for understanding the underlying mechanisms of observed trends, the remote-sensing based trend estimates are more relevant for informing the construction of the counterfactual in our study.
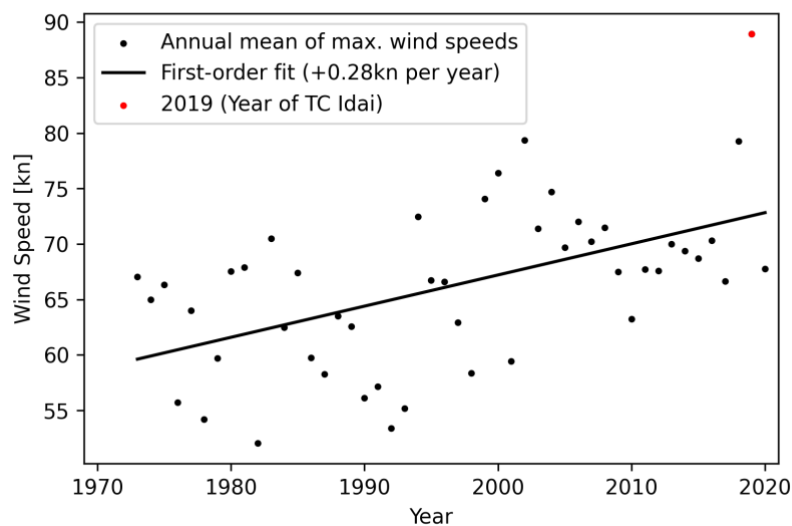
Figure 2: Annual means of maximum TC wind speeds in the South Indian Ocean (maximum 10-minute sustained wind speeds). Linear trend over the period 1973-2020; data from IBTrACS database (Knapp et al., 2010).

2.2 Coastal Flood Modeling

The storm surge flood simulations are generated using the open-source geophysical flow solver GeoClaw (Mandli and Dawson, 2014). GeoClaw uses an efficient adaptive mesh refinement to model wind- and pressure-induced wave dynamics in the 2-dimensional depth-averaged shallow water equations. The input data includes TC tracks, astronomical tides, and topographical raster data (see below) and GeoClaw provides outputs in the form of gridded maps of maximum flood heights as well as the temporal dynamics of storm surge at virtual tide gauge locations. We configure GeoClaw to limit the automatic mesh refinement to a spatial resolution of between 1 and 8 arc-seconds (approximately 30 and 240 m) inside of Idai's landfall area and to between 100 and 900 arc-seconds (approximately 3 and 27 km) in the open ocean.

As the factual input for GeoClaw, the TC track data from IBTrACS (Knapp et al., 2010) provided by the WMO Regional Specialised Meteorological Center at La Reunion (operated

by MeteoFrance) is used. For the counterfactual scenarios with modified TC intensity, we multiply all wind speed values along the track by a scalar factor of 0.9 (for a decrease of 10% in intensity). The central pressure at each track position is increased by 0.1 times the difference between central pressure and environmental pressure.

From the wind speed, pressure, and radius information provided along the TC track, GeoClaw derives surface wind speeds and air pressure at arbitrary locations in space and time using a radially symmetric wind profile (Holland, 1980) combined with the influence from the storm's translational speed.

GeoClaw does not incorporate any tidal dynamics, nor meteorological forcings apart from the TC wind and pressure fields mentioned above. To account for the influence of astronomical tides, we configure GeoClaw to use an initial sea level according to gridded satellite altimetry for 2019 (CMEMS, 2021), optionally enhanced by the minimum, mean, or maximum simulated astronomical tides in the region of landfall according to the FES2014 global ocean tide atlas (Lyard et al., 2021). For the counterfactual sea level scenarios, the amount of sea level rise specified in the scenario description (between 6.5 and 17.0 cm) is subtracted from the initial sea level.

The topographical input for GeoClaw is taken from digital elevation models (DEMs). We use a combination of CoastalDEM 2.1 (Kulp and Strauss, 2021, 2018) in coastal areas, SRTM 15+ V2.3 (Tozer et al., 2019) over the open ocean and Multi-Error-Removed Improved-Terrain (MERIT) DEM) (Yamazaki et al., 2019) everywhere else. All datasets are converted to the same geoidal vertical datum (EGM96) at a spatial resolution of 9 arc-seconds (approximately 300 m). This resolution is the highest resolution where we were able to obtain numerically stable results from GeoClaw. We note that no harmonization has been applied to make up for disagreements between the different DEM products so that the transition from CoastalDEM topography to SRTM 15+ bathymetry can be steep.

Due to a lack of tide gauges or suitable observed flood extent in Mozambique, it is not possible to validate the performance of GeoClaw for TC Idai in the factual model runs. However, we compare the water levels at a virtual tide gauge station off the coast of Beira, where the highest impacts from TC Idai have been reported, with simulated water levels from the Global Tide and Surge Model (GTSM) (Dullaart et al., 2021; Muis et al., 2020), and find the best agreement of maximum surge heights for the GeoClaw run with the maximum astronomical tide assumption, closely followed by the run assuming the monthly mean sea level (no tidal adjustment) (Supplementary Figure S1).

2.3 Inland Flood Depth Estimation

Gridded depth maximums for the flood event (Supplementary Figure S2) is calculated using the Rolling HAND Inundation Corrected Depth Estimator (RICorDE) tool(Bryant et al., 2022) supplied with terrain data from the MERIT DEM project, permanent surface water data from the Joint Research Centre (JRC) Global Surface Water project (Pekel et al., 2016), and flood extents from the FloodScan product (Atmospheric and Environmental Research & African Risk Capacity, 2022). MERIT DEM provides a roughly 90 m resolution global layer derived from multiple space-based sensors to minimize elevation errors. The maximum water extent layer

274 from JRC's Global Surface Water project provides a roughly 30 m resolution global layer of
275 locations detected as inundated on Landsat imagery (Wulder et al., 2016) from 1984-2019
276 (Pekel et al., 2016). Observed flood extents for TC Idai are obtained from Atmospheric and
277 Environmental Research & African Risk Capacity's accumulated 2-tier standard flood extent
278 depiction FloodScan product from 2019-03-01 to 2019-03-31 using the MERIT DEM
279 resolution. Originally developed for applications in Africa, this FloodScan algorithm relies on
280 satellite based low-resolution passive microwave data and was designed to capture national-
281 scale events. To accomplish this, the algorithm minimizes false-positives, making the
282 algorithm more prone to false-negatives and less sensitive to events with smaller spatial extent
283 and urban floods (Galantowicz and Picton, 2021). All data layers are re-projected to 90 m
284 resolution geodetic coordinates prior to the RICorDE computation.

286 RICorDE is a tool developed in pyQGIS for post-event analysis of fluvial flood events using
287 inundation masks derived from space-based observations. RICorDE first generates a Height
288 Above Nearest Drainage (HAND) grid followed by an inundation correction phase and a water
289 surface level (WSL) calculation phase. As part of pre-processing, the HAND grid is obtained
290 using WhiteboxTools' *ElevationAboveStream* (Lindsay, 2014) from the permanent surface
291 water layer and the DEM. In the first phase of RICorDE, the observed flood extents are
292 hydraulically corrected to account for under-predictions using the permanent surface water
293 layer and over-predictions using a HAND-derived inundation representing the upper quartile
294 of possible flooding extents. In the second phase, HAND values sampled from the inundation
295 shoreline are used to produce an interpolated WSL grid using WhiteboxTools' CostAllocation
296 algorithm (Lindsay, 2014). Finally, gridded water depths are obtained from this WSL grid
297 through subtraction with the DEM. RICorDE is explained in detail in the tool publication (Bryant
298 et al., 2022) and the source code can be accessed online
299 (https://github.com/NRCan/RICorDE/tree/main).

301 The slower, more complex RICorDE algorithm has been shown to produce more accurate
302 depths maps for two fluvial flood events in Canada when compared to faster, more disaster
303 response-focused solutions like the Floodwater Depth Estimation Tool (FwDET) (Bryant et al.,
304 2022; Cohen et al., 2018). While no data is available to validate the performance of the depths
305 estimate for TC Idai, visual inspection suggests results are less accurate in areas with higher
306 elevation (>20 m), especially where drainageways are of comparable width to the resolution
307 of the JRC water extent layer. These false negatives in the JRC layer propagate as positive
308 bias in the HAND routine, which leads to higher elevation water surface predictions and similar
309 positive bias in the depth values (see white arrow in Figure S3a).

2.4 Combined Flood Depth Product

311 The inland flood depth estimates from RICorDE are resampled from 3 arcsec to 9 arcsec,
312 using the average resampling method (Rasterio library for Python), to match the resolution of
313 the GeoClaw output. All flood depths are rounded to the nearest decimeter, their outline is
314 cropped to the area of interest, and the final factual flood depth in each grid cell (shown in
315 Figure 3a) is determined as the maximum of both products. This accounts for both potentially
316 partly obscured satellite imagery by clouds and potential underestimation by the numerical
317 model.

$$d_0 = max \left(d_{c,0}, d_r \right) \qquad (1)$$

with d_0 referring to the factual flood depth, and indices c and r referring to the coastal flood model (GeoClaw) and to the remote sensing data translated into flood depth using RICorDE, respectively. To derive the counterfactual flood depth d_{cf}, we subtract the difference between modeled factual and counterfactual coastal flood depths from the combined factual flood depth:

$$d_{cf} = d_0 - \left(d_{c,0} - d_{c,cf} \right) \qquad (2)$$

2.5 Displacement

We use displacement data from the publicly accessible GIDD, maintained by the *Internal Displacement Monitoring Centre* (IDMC, 2022). IDMC follows the definition of displacement provided in the *Guiding Principles on Internal Displacement* (OCHA, 2004), which states that "[i]nternally displaced persons are persons or groups of persons who have been forced or obliged to flee or to leave their homes or places of habitual residence, ... and who have not crossed an internationally recognized State border". This definition covers permanent displacement, temporary displacement, and pre-emptive evacuations (Gemenne, 2011), all summarized as "displacements" within our study. No granular information is available in GIDD on the type of displacement. Displacement numbers are based on multiple secondary sources, such as IOM, OCHA, or - in the case of TC Idai - the Mozambique National Institute of Disaster Management. The TC Idai event is categorized as a "storm" event, however, no information is given on how many of the displacements were caused respectively by flooding, strong winds, or a combination of both. Because of the extensive flooding observed in the wake of Idai's landfall and humanitarian reports often focused on flooding (ReliefWeb, 2019a), we assume in our main analysis that all displacements are caused by flooding (either coastal or inland). We assume that people exposed to flood levels greater or equal than 100 cm are affected by the flooding and thus prone to displacement, following previous studies (Custer and Nishijima, 2015; Kam et al., 2021). However, we also test the sensitivity of our results to this threshold choice by evaluating alternative water level thresholds of 10 cm and 50 cm. Our modeling approach assumes an artificially deterministic link between the TC hazard and displacement, which is adequate in the context of the factual-counterfactual approach where only one parameter - storm surge hazard - is modified while everything else, including vulnerability, is held constant. In general, the relationship between climatic events, pre-existing socio-economic conditions, and displacement is complex and only partially understood (Cattaneo et al., 2019; UK Government Office for Science, 2011). In other words, our study addresses the question of how many displacements might have occurred in a different climate but with the same vulnerability as observed; it does not address the question of how this vulnerability came about.

We first determine the flood extent with depths greater than the selected water level threshold and overlay it with population data to estimate the number of people affected. We use gridded population data from GHS-POP (Schiavina et al., 2019) for the year 2015, on 9 arcsec resolution. Population growth in Mozambique was 1.12 % between 2015 and 2019 (The World

363   Bank, 2022); we hence multiply all population grid cells with this factor, assuming a spatially
364   equal population growth.
365
366   We then calculate the ratio between the number of observed displacements, and the number
367   of affected people from the factual flood estimate. This ratio, which may be thought of as an
368   event-specific displacement vulnerability factor, is different for every tide assumption,
369   reflecting the uncertainty about the actual flood extent and depth. We compute for every
370   impact level threshold i and tide assumption h a displacement vulnerability factor $v_{i,h}$ by
371   dividing the number of observed displacements D_o by the total number of affected people of
372   the factual scenario $A_{i,h,o}$:

$$v_{i,h} = \frac{D_0}{A_{i,h,0}} \qquad (3)$$

376   Multiplying the specific displacement vulnerabilities with the counterfactual numbers of
377   affected people, we derive the number of people at risk of displacement in a world without
378   climate change. This means that the difference between factual and counterfactual
379   displacement estimates comes only from differences in the flood hazard, while exposure and
380   vulnerability factors are held fixed. We achieve this by multiplying $v_{i,t}$ with the number of
381   affected people of the counterfactuals $A_{i,h,cf}$, and estimate the expected number of
382   displacements for each counterfactual scenario $D_{i,h,cf}$:

$$D_{i,h,cf} = v_{i,h} * A_{i,h,cf} \quad (4)$$

386   We point out that the use of predefined flood thresholds implies the assumption that at a given
387   flood depth, the risk of severe damages to, or even destruction of, residential buildings and
388   other infrastructure typically becomes so large that people *may* be forced to flee. The number
389   of people that *actually* become displaced then depends on additional physical, political and
390   socio-economic factors, which may vary between local contexts and are not generally known.
391   Their aggregate effect is reflected in the specific vulnerability factor $v_{i,h}$. In other words, the link
392   between flood hazard and displacement is "soft" in the sense that it is mediated by the local
393   vulnerability. An alternative assumption would be that there is an (event-specific) flood-depth
394   threshold below which there is no displacement, and above which people become displaced
395   regardless; that is, a "hard" link between flood hazard and displacement. In this case, the
396   flood-depth threshold could be derived directly from the data, as the depth level at which the
397   calculated number of affected people equals the reported number of displacements. When we
398   sum up the affected people per 10 cm flood depth increment for TC Idai, we obtain a threshold
399   of about 400 cm (similar for all tide assumptions; Supplementary Table S1), for which the
400   modeled number of affected people approximately equals the number of observed
401   displacements. This value is very high in comparison with the thresholds cited further above,
402   and we believe it is implausible for displacement to occur only in locations inundated by 4
403   meters or more. This exercise therefore lends further justification for the "soft link" approach.
404
405   Even though disaster reports for TC Idai suggest flooding to be the main driver of
406   displacement, high wind speeds may have locally intensified the impact of TC Idai (Figure S4)
407   and be partially responsible for the observed displacements. We conduct an additional
408   analysis where we assume that people affected by either flooding or wind (or both) were at
409   risk of displacement with an equal vulnerability factor. We use a wind speed threshold of 96

410 kn (50 m s⁻¹) for population exposure (Geiger et al., 2018), corresponding to the Saffir–
411 Simpson scale classification 3 (major hurricane). The resulting wind field is overlaid with
412 gridded population data to compute the number of affected people, excluding those who are
413 already affected by flooding.

414 3 Results

415 3.1 Simulated flooding

416 We calculate storm surge flood extent and depth for the factual (driven with observed wind
417 speeds and sea levels) and counterfactual (reduced wind speeds and sea level) scenarios.
418 The difference between factual and counterfactual flooding (maximum tide, 10.5 cm SLR, 10%
419 TC intensification) is illustrated in the densely populated area of Beira (Figure 3b), the city
420 where TC Idai made landfall and destroyed 90% of all houses according to some disaster
421 reports (ReliefWeb, 2019b). Beira consists of two major population centers, of which the
422 southern one is close to the seaside and exhibits a higher population count.

424 Both factual and counterfactual flood extent covers the southern, highly populated part of Beira
425 (Figure 3c and 3d). The northern parts of the city are only marginally affected. Flood extents
426 are also similar between factual and counterfactual simulations in the areas east of Beira and
427 around the inflow of the Buzi River, located on the opposite side of the bay. Only a few isolated
428 locations no longer experience flooding after removing the effects of climate change.

430 In contrast, differences in simulated flood depth are more pronounced (Figure 3e).
431 Counterfactual flood depths are up to 80 cm lower than factual flood depth in some parts of
432 the southern city center. The highest difference in flood depth, of up to 140 cm, is found
433 between the northern and southern population centers of Beira. Flood depth differences
434 outside of Beira are rather low, however, Figure 3c and 3d show that absolute flood depths
435 drop below the critical flood depth of 100 cm over great parts around the west bank of the
436 Pungwe River inflow. Overall, it is observable that depth differences (between factual and
437 counterfactual simulations) are higher in less populated parts, especially in Beira. This could
438 partly result from the fact that digital elevation models tend to overestimate elevation in dense
439 urban settings (Shen et al., 2019), thereby underestimating flood depth and potentially also
440 differences in flood depth between different scenarios, however, this is hard to ascertain given
441 the available data. Nonetheless, local variations in simulated flood depth should be interpreted
442 with care.

443
444
445
446
447
448
449
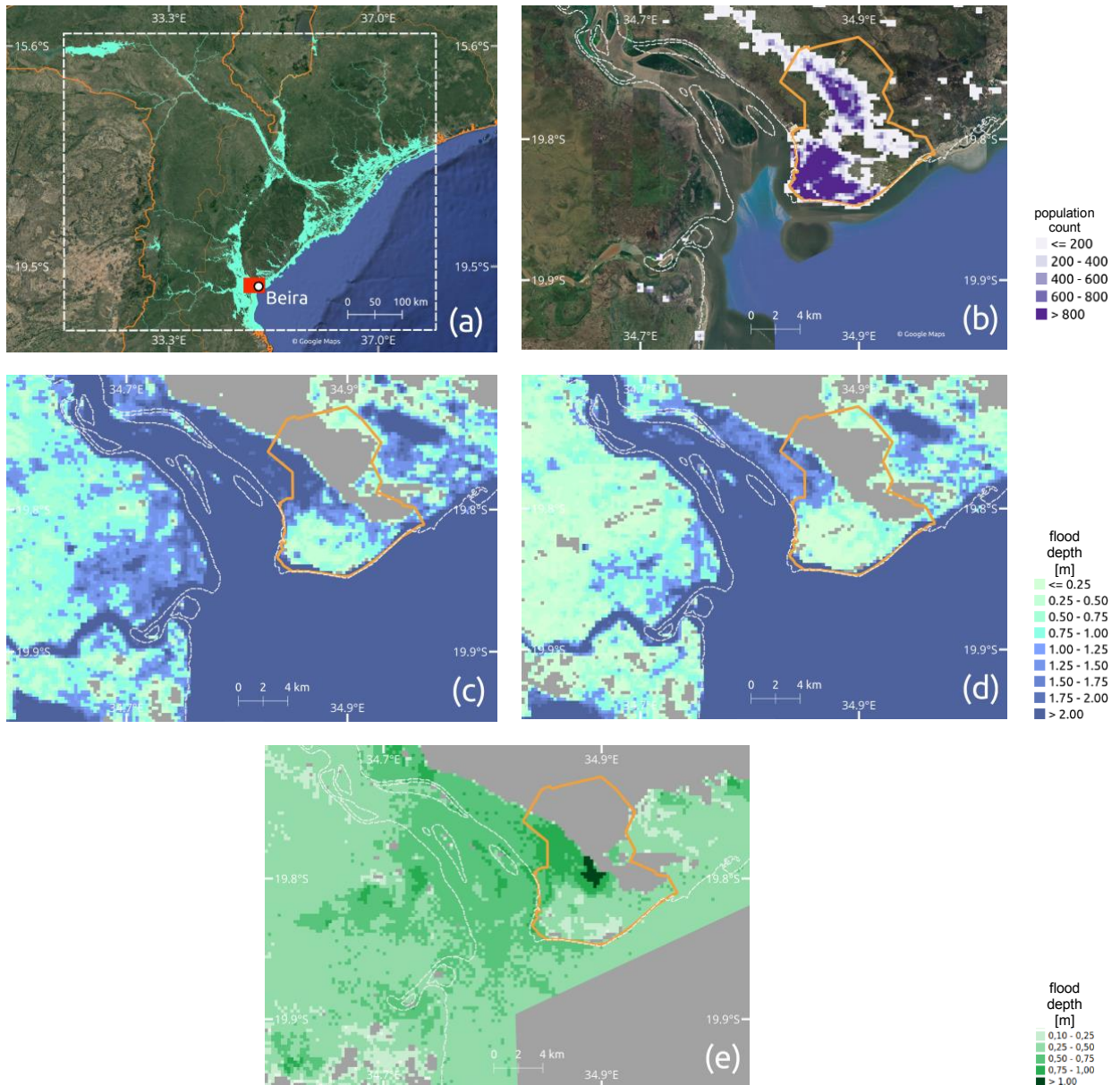
Figure 3: Simulated flood extent for Mozambique; population distribution and inundation levels for the greater area of Beira. (a) Combined factual estimate of inland and coastal flooding (binary; flood/no-flood). White dashed box shows the area of interest in which flood exposure is computed. Red rectangle shows the extent of the section displayed in panel (b) - (e). (b) Population distribution for the greater area of Beira. Flood extent and levels for (c) the factual scenario (max. tide), and (d) the "counterfactual TC intensity + sea level rise (10.5 cm) - max. tide" scenario. Flood depth difference between (c) and (d) is displayed in (e). City neighborhoods of Beira (HDX, 2019) are indicated by orange lines and shoreline (Wessel and Smith, 1996) is represented by dashed white lines in (b) - (e); satellite image background by © Google Maps (Google Maps (b), 2022) in (a) and (b).

3.2 Displacement

In the next step, we investigate how the factual and counterfactual flood estimates translate into population at risk of displacement for the whole of Mozambique. We compare factual and

counterfactual affected people/displacements and compute the absolute relative change based on the counterfactual results, representing the increase in impact due to climate change. Our analysis shows that the intensification of TC wind speeds leads to an increase in flood affected people and, consequently, in displacements by up to 2.7%, while counterfactuals regarding the sea level lead to only small changes by up to 1.3 % (Figure 4, Table 1 and Table S2). A combination of both counterfactuals only slightly exceeds the range (increase by up to 3.2% for the maximum tide assumption) as in contrast when considering the TC intensification alone. Despite the large uncertainty regarding SLR since 1900, the difference in the number of people affected (or displaced) is rather marginal; being less than 1% increase between the largest and the smallest SLR estimate for the "cf SLR" simulations. Our results highlight that the tide assumption plays a major role. The minimum and mean tide lead to marginal changes in affected/displaced people, in contrast to the maximum astronomical tide and monthly mean sea level from satellite altimetry (no tide), which show for the "cf SLR + wind" simulations a median change in 3.0% (maximum change in 3.2%) and 2.7% (3.2%), respectively. Given the high number of affected people, already small changes in the counterfactual scenarios lead to high changes in absolute numbers. The coupled effect of higher wind speeds and higher sea level increases the number of affected people and displacements by up to 39,300 and 14,900 (maximum tide) and 38,100 and 14,600 (monthly mean), respectively. Results regarding impact flood levels of 10 cm and 50 cm are displayed in Table 1 and the supplementary material (Figure S5 and S6), showing even higher changes for the counterfactual scenarios of up to 56,500 displacements (13.4% increase).

Besides our central TC intensification assumption of 10%, we also examine two alternative assumptions of 8.5% and 12% intensification, respectively, for the "max" tide (Figure 5). The spread among the intensification scenarios is rather small, with median relative changes varying between 2.9% and 3.7%. This translates to median estimates of 35,300 and 44,600 affected people, or 13,400 and 16,900 displacements, respectively (Table 1 and Table S2). In contrast, the difference between the highest (4.0%) and lowest values (2.2%) is larger. In absolute terms, this means a range of between approximately 27,400 and 48,200 affected people, or 10,400 and 18,200 displacements.

We assume that high wind speed caused only a marginal fraction of displacements, following disaster reports, media coverage and experience from other events; as an extreme example, wind by Hurricane Sandy caused less than 0.01% of the overall damage (Strauss et al., 2021). Nonetheless, in an additional sensitivity analysis, we also account for the number of people affected by high TC wind speeds of 50 m s^{-1} or above (Sect. Methods). Our analysis reveals that the number of people affected not by flooding (maximum tide assumption, 100 cm impact threshold) but by high wind speeds ranges between 340,900 to 360,600 in the factual simulation. In the counterfactual, even the maximum wind speed attained in any grid cell outside the flooded area drops from 51.5 m s^{-1} to 46.3 m s^{-1}, i.e. below the above-mentioned threshold; thus, no people are counted as affected. Assuming the same vulnerability factor for displacement due to high wind speed as due to flooding yields i 103,700 to 112,100 displacements, or 21.7 to 23.4% of the total displacement, attributable to climate change.

512

513

514
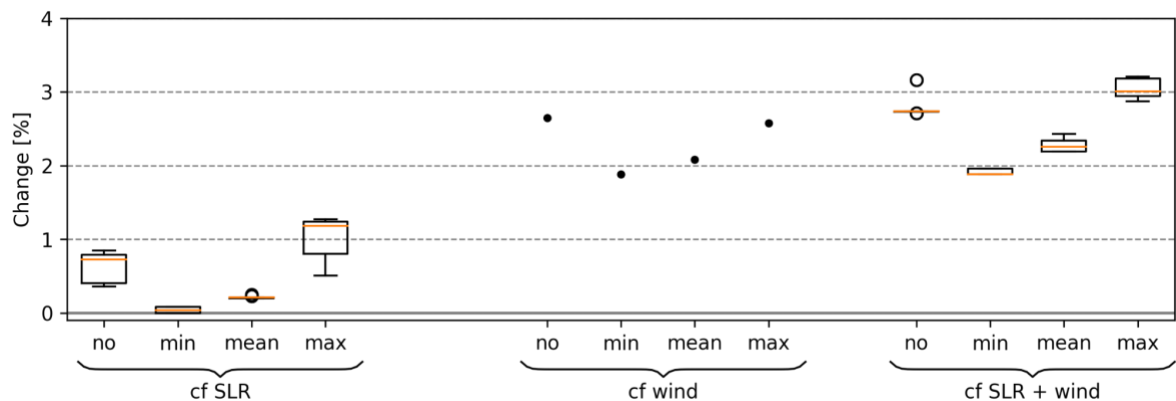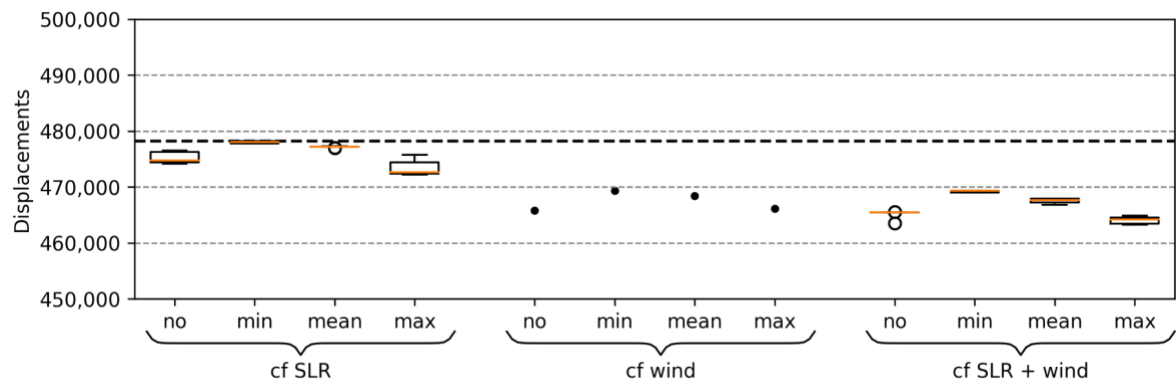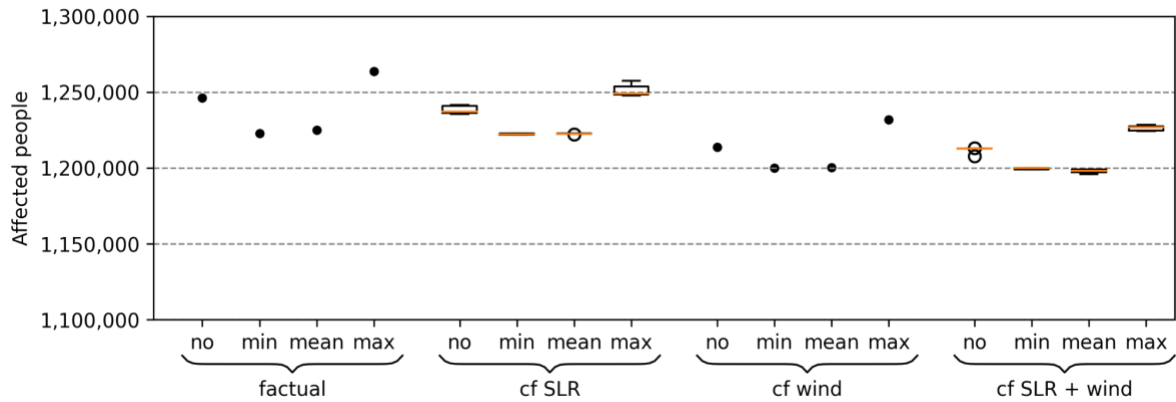
Figure 4: Simulated affected people (top), displacements (middle) and percentage change (bottom) for the 100 cm impact threshold. The percentage change compares factual and counterfactual displacements, and represents the absolute relative change based on the counterfactual results. Three counterfactual scenarios are shown: lower sea level ("cf SLR")), intensification ("cf wind"), and a combination of both ("cf SLR + wind"). Additionally, a variety of counterfactual sea levels as well as a set of astronomical tides is presented, covering minimum ("min"), mean ("mean"), and maximum ("max") as well as monthly mean sea level from satellite altimetry ("no"). Bold dashed line in the middle panel shows the number of

14

observed displacements. Percentile changes in affected people and displacements are the same. The second quartile Q2 (median) of the box plot is shown in orange, "whiskers" are placed at ±1.5 * interquartile range (Q3-Q1).

Table 1: Overview main results for modeled displacement impact. Min./Median/Max. are related to the SLR scenarios. Orange background of the first results row indicates the primary parameter estimate. Cells with gray background indicate the altered parameter in comparison with the primary estimate.

Counterfactual	Flood-Depth Threshold [cm]	Intensification [%]	Tide	Displacements Dif. Min.	Displacements Dif. Median	Displacements Dif. Max	Displacements Dif. Min. [%]	Displacements Dif. Median [%]	Displacements Dif. Max [%]
SLR + wind	100	10	max	13331	13958	14875	2.9	3.0	3.2
SLR + wind	100	10	no	12620	12740	14629	2.7	2.7	3.2
SLR + wind	100	10	min	8822	8822	9183	1.9	1.9	2.0
SLR + wind	100	10	mean	10235	10543	11353	2.2	2.3	2.4
SLR + wind	50	10	max	46695	49336	52275	10.8	11.5	12.3
SLR + wind	10	10	max	28557	32218	34456	6.4	7.2	7.8
SLR	100	10	max	2407	5584	5981	0.5	1.2	1.3
wind	100	10	max	-	12033	-	-	2.6	-
SLR + wind	100	8.5	max	10384	13354	14321	2.2	2.9	3.1
SLR + wind	100	12	max	14297	16870	18232	3.1	3.7	4.0
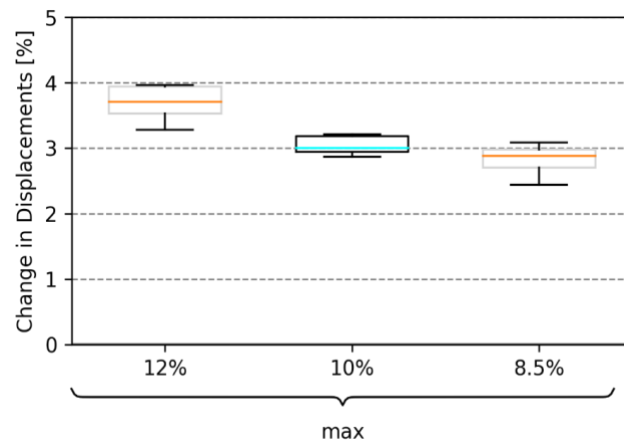
Figure 5: Percentage change in displacements between factual and counterfactual, for three different TC intensification assumptions. The percentage change compares factual and counterfactual displacements, and represents the absolute relative change based on the counterfactual results. The combined counterfactual scenario ("cf SLR + wind") with 100 cm impact threshold and the maximum astronomical tide ("max") is displayed. The central assumption of 10% intensification is highlighted with a cyan-colored median in the box plots. The second quartile Q2 (median) of the box plot is shown in orange/cyan, whiskers are placed at ±1.5 * interquartile range (Q3-Q1).

4 Discussion and conclusions

With more than one degree of global warming, most, if not all, extreme weather events now can be assumed to bear some imprint of climate change. By extension, this is also true for the humanitarian crises induced by catastrophic storms, floods, or droughts. However, while economic damages from climate change have been attributed both in case studies and global

studies (Frame et al., 2020b, 2020a; Sauer et al., 2021; Strauss et al., 2021), little is known about the extent to which climate change has already exacerbated human displacement. Our modeling study of TC Idai suggests that climate change may have induced between 12,600 (2.7%; lowest estimate under the no tide assumption) and 14,900 (3.2%; highest estimate under the maximum tide assumption) additional displacements from this one event. This is primarily due to the intensification of TC wind speed inducing a more powerful storm surge; and to a lesser extent due to sea level rise providing a higher baseline for the storm surge. We also show that the sensitivity of the results to the choice of TC intensification is approximately in the same range as for the tide assumption. We note that our attribution statements are, as commonly in the climate (impacts) attribution literature, purely statistical; that is, we do not make any claims about whether or to what extent any individual person may have been displaced because of climate change. Our methodology and results are subject to a variety of limitations and uncertainties, primarily related to the models (coastal, fluvial, DEM) and underlying datasets (population, displacement). Additional sources of uncertainty are the counterfactual input quantities (SLR, wind speed intensification), impact flood levels, and tide assumption, for which we perform sensitivity analyses.

Our results likely underestimate the full contribution of climate change to displacement associated with TC Idai, because we solely addressed the effect of climate change on coastal flooding, neglecting changes in inland flooding. Between March 3 and 17, heavy precipitation between 200-400 mm was registered for Beira City and the region, with upstream sections of the Pungwe River basin exposed to more than 600 mm (Probst and Annunziato, 2019). With growing evidence that climate change not only affects precipitation intensity (Fowler et al., 2021; Guerreiro et al., 2018; Scherrer et al., 2016) but also continental-scale changes in fluvial flood discharge (Blöschl et al., 2019; Gudmundsson et al., 2021), it is likely that in a world without climate change, the river flood magnitude would have been smaller, and even less people would have been exposed than in our coastal-only counterfactual. Quantifying this additional effect would require a river flood model capable of reproducing the observed flood extent and associated inundation depths, and ideally coupled with a coastal flood model to capture the interaction between river flood and storm surge. Even though globally-applicable frameworks for compound flood hazard modeling are under construction, and have recently been tested for TC Idai (Eilander et al., 2022), evaluations of fluvial flood models reveal important shortcomings in data-scarce regions such as Mozambique (Bernhofen et al., 2018; Mester et al., 2021). Quantifying the role of river flooding in TC-induced displacement thus is a timely challenge.

The inland river flood estimates based on satellite imagery exhibit several limitations and uncertainties. In the absence of validation data, it is difficult to quantify the uncertainty arising from the inland flood depths estimation. These gridded values are highly sensitive to the input layers, namely the DEM (MERIT), permanent surface water (JRC), and the satellite-based observation of inundation extents (FloodScan) (Atmospheric and Environmental Research & African Risk Capacity, 2022). Especially uncertainties regarding the choice of DEM, used for both the inland flood depth estimation and the coastal flood model, should not be neglected (Hawker et al., 2018). Qualitatively, the performance seems poor in areas with higher elevations (>20m). This could be attributable to challenges in representing the topography at 90 m resolution and dense obstructions that scatter returning signals (Shen et al., 2019).

594 Similarly, no suitable validation data for the coastal flood simulations is available. According
595 to the FloodScan description (Atmospheric and Environmental Research & African Risk
596 Capacity, 2022), the used products "depict large scale, inland river flooding well but are less
597 likely to depict flooding in smaller floodplains and near coastlines". We have hence opted to
598 not choose the FloodScan product as the sole coastal flood hazard estimate nor as validation
599 dataset for the flood extent from our coastal flood model. A flood risk screening for Beira (van
600 Berchum et al., 2020) showed that simulated flood extent for a 10-year rainfall event plus a
601 10-year coastal surge event covers most parts of the Central and Munhava city districts of
602 Beira (South-Eastern city districts). In contrast, the FloodScan product shows only little
603 flooding in this area, while it is assumed that flooding by TC Idai exceeded an average
604 recurrence interval of 10 years. For example, Emerton et al. (2020) show that GloFAS flood
605 forecasts indicated a 100% probability of exceeding the severe flood alert threshold (20-year
606 return period) for TC Idai at the Pungwe River (Emerton et al., 2020). Furthermore, newspaper
607 photographs (Bergensia, 2019) show flooding in the Area de Baixa part of Beira (Western
608 district of Beira), which was only partially flooded according to the satellite imagery. The AER
609 product thus likely underestimates flood extent, which   may be explained by cloud
610 obscurement or failure in automatic flood detection due to, for example, flooding in densely
611 populated areas, or the satellite passing over some time after the peak flooding when water
612 levels have already receded.

614 Furthermore, the coastal flood modeling framework does not incorporate any astronomical
615 tidal dynamics. Because there are no tide gauge records available in the region, we were only
616 able to compare the model's surge heights to the state-of-the-art Global Tide and Surge Model
617 (GTSM). For the derived flood maps, there were no observational benchmarks available for
618 validation. Moreover, the model is not able to take the interaction of the coastal surge with
619 increased river discharge at the estuaries into account. In some cases, this interaction has
620 been shown to influence water levels in a nonlinear way, for example for the 2016 Louisiana
621 flood (Bilskie and Hagen, 2018). Another source of uncertainty is again the DEM, in particular
622 the transition from topographic to bathymetric data at the coast lines.

624 Additionally, our analysis may be sensitive to the choice of population dataset (Archila Bustos
625 et al., 2020; Leyk et al., 2019), which may lead to uncertainties regarding our estimated
626 exposure. One of the main error sources for population datasets is related to the areal
627 interpolation methods to disaggregate the population data (Archila Bustos et al., 2020). GHS-
628 POP distributes population only within built-up areas, which has the downside that non-
629 residential areas are simulated as populated as well (Freire et al., 2016). In fact, a comparison
630 with satellite imagery reveals that some areas in Beira are populated which are most likely
631 only commercial or industrial sites. On the other hand, not all settlements are captured by
632 GHS-POP, most likely due to their building type. Nonetheless, GHS-POP is still one of most
633 accurate datasets in estimating and modeling the known population (Archila Bustos et al.,
634 2020), especially in urban contexts (Leyk et al., 2019) as in the case for Beira.

636 No information is available regarding the spatial distribution of displacements within GIDD; we
637 assume that vulnerability to displacement is uniform across the affected area. The total
638 number of displacements is furthermore not specifically categorized by hazard type, which
639 reflects the multivariate (wind, rain and flood) compound characteristic of TCs hazards
640 (Zscheischler et al., 2020). However, this impedes the attribution of coastal flood-induced
641 displacements. Furthermore, the GIDD estimates include different forms of displacement,

642 such as forced displacement or pre-emptive evacuations, with the latter potentially accounting
643 for a substantial proportion (McAdam, 2022). This poses far-reaching implications for
644 displacement risk modeling, as evacuations may already be triggered by lower flood depths,
645 or by early warnings of an impending hazard, which may not materialize in the expected
646 manner, or may not cause the level of destruction that would lead to a corresponding
647 magnitude of forced displacement.

649 Our main analysis also assumed no direct effect of high wind speeds on displacement, lacking
650 clear evidence for substantial displacement due to high winds alone. Our additional sensitivity
651 analysis suggests that changing this assumption could increase the number of displacements
652 attributable to climate change considerably. Given this potentially large effect, and our limited
653 understanding of the relative roles of different drivers of displacement in general, the specific
654 vulnerability to displacement from different types of hazard should be the subject of future
655 studies. Moreover, assuming that displacement can occur already at inundation depths of less
656 than 100 cm also leads to higher estimates of climate change-attributable displacement,
657 according to our sensitivity analysis. We also tested if the flood-depth threshold can be
658 estimated from the data by summing up the affected people per 10 cm flood depth increment
659 until equaling the number of observed displacements. This analysis yields an alternative flood-
660 depth threshold of 400 cm, which we assess to be physically not reasonable in the context of
661 building structure in Mozambique. Again, a better understanding of vulnerability beyond hard
662 physical flood-depth thresholds and empirically derived vulnerability factors will be critical to
663 refine risk assessments. Future work may produce a functional relationship between
664 displacement risk, contextual drivers, and physical flood properties, covering, for example,
665 depth, velocity, and duration.

667 We did not change storm track or size in our counterfactual simulations. While storm tracks
668 may be affected by climate change (Knutson et al., 2019), we assume that Beira has not
669 become more or less likely as a landfall site. Mean storm size is found to increase
670 systematically with the relative sea surface temperature (Chavas et al., 2016), although
671 numerical simulations suggest that projected median sizes remain nearly constant globally
672 (Knutson et al., 2015). Assuming increases in storm size due to climate change would again
673 result in higher estimates of attributable displacements in our analysis. By design, in our
674 attribution study, we assumed a fixed population distribution in both factual and counterfactual
675 simulations, as well as a fixed, empirically determined displacement vulnerability factor, and
676 only investigated changes in displacement risk following from changes in the physical
677 characteristics of TC Idai and its impacts. Assessments of future risks - or of past impacts -
678 should not only take into account the intensification of physical hazards, but also changes in
679 exposure (Kam et al., 2021); as well as potential changes in vulnerability due to social,
680 economic, or technological developments. For instance, TC-related displacements depend not
681 only on the damage to housing, but also on other factors such as government responsiveness
682 or poverty levels (Cissé et al., 2022). Here, we have chosen a storyline approach for the impact
683 attribution instead of a more traditional probabilistic attribution approach (Philip et al., 2020;
684 Titley et al., 2016), as for instance previously employed to attribute heavy precipitation of
685 Hurricane Harvey (Oldenborgh et al., 2017) to climate change. One reason is that for
686 Mozambique neither the complete time series of rainfall nor the high station density required
687 by a probabilistic approach (van Oldenborgh et al., 2021) are available. Reanalysis products
688 for precipitation could be used as an alternative, however, their quality depends on geographic
689 location, so the use of multiple reanalysis and/or observation products is recommended

690 (Angélil et al., 2016). Nonetheless, a climate attribution approach focusing on changes in the
691 probability or intensity of TCs in the South Indian Ocean due to anthropogenic forcing (O'Neill
692 et al., 2022) could guide the construction of counterfactual scenarios of the storyline approach.
693 Further, in contrast to the probabilistic approach, the storyline approach allows us to
694 investigate the driving factors involved, as well as their plausibility (Shepherd et al., 2018).

696 Framing the risk of tropical cyclones in the context of climate change in an event-specific rather
697 than a probabilistic manner also allows us to assign absolute numbers of attributable
698 displacements, which raises risk awareness in a more tangible way. Even though these
699 numbers include substantial and important uncertainties related to the models, datasets and
700 counterfactual assumptions, as discussed above, they provide an informative quantitative
701 indication of the additional risk posed by climate change to communities affected by one of
702 the worst natural disasters in recent history. The responsibility for managing and reducing
703 displacement risk lies primarily at the national and provincial level, but often local authorities,
704 organizations, and communities respond to displacement disasters (Hollinger and
705 Sienkevych, 2019). Demonstrating quantitatively how climate change affects the societal risks
706 associated with natural hazards may play an important role in raising awareness, with different
707 types of stakeholders, to the changing nature of such risks. It may also incentivize
708 governments to step up their efforts both in terms of planning and investing into adaptation
709 measures, and rapidly mitigating greenhouse gas emissions. The storyline approach is
710 particularly suited for highlighting the risk-amplifying effects of climate change in a tangible
711 and accessible way, based on a well-known event in the recent past (van den Hurk et al.,
712 2023). Estimates of the costs of displacement additionally highlight the adverse economic
713 aspects of climate change (Desai et al., 2021); average costs have been put at $310 per
714 displaced person per year, though actual costs are heavily dependent on the country and
715 duration (days/weeks to years) (IDMC, 2019). Only 50.7% of the required Mozambique
716 Humanitarian Response Plan 2019 of US$m 620.5 was funded, demonstrating that climate
717 change poses an additional burden to insufficiently equipped financial aid resources.
718 Anticipating the intensification of tropical cyclones under future global warming (Knutson et
719 al., 2020) calls for enhancing adaptation measures as well as disaster relief and humanitarian
720 aid. The IPCC AR6 projects an additional global increase in mean sea level and surface
721 temperature of 0.44 m / 1.2°C (SSP1-2.6) and 0.77 m / 4.0°C (SSP5-8.5), relative to a baseline
722 of 1995-2014, by the end of the 21st century (Fox-Kemper et al., 2021; Lee et al., 2021). Even
723 though these increases may vary between basins, an enhanced displacement risk due to Idai-
724 like TCs needs to be accounted for in the next decades, especially if future changes in
725 exposure due to population growth and urbanization are considered. Under both SSPs 1 and
726 5, the population of Mozambique is projected to increase by approximately 8 million, and its
727 urbanization level from about 40% to over 70%, just over the next 30 years (Riahi et al., 2017).

729 Our study expands the scope of extreme event impact attribution to include displacement as
730 a societal impact dimension. In general, due to the lack of calibrated regional models and
731 gauge stations, only few attribution studies (Luu et al., 2021; Takayabu et al., 2015) focus on
732 storms - or any extreme weather events, for that matter - in low-income countries. This not
733 only limits our understanding of climate change effects on extreme events from a global
734 perspective, but also biases geographically the amount of knowledge and information
735 available to inform risk management and adaptation strategies (Otto et al., 2020). Our impact
736 attribution is built on global-scale datasets and models, which could be employed in other
737 relevant locations. Despite the discussed limitations and uncertainties inherent to this

738 approach, displacements could be similarly attributed to climate change for other major TCs
739 that occurred in data- and model-scarce regions, such as Typhoon Haiyan (Philippines; 4.1
740 million displacements) or Cyclone Amphan (India and Bangladesh; combined 4.95 million
741 displacements) (IDMC, 2022). The continuing increase in spatial resolution of global-scale
742 products will eventually allow for more granular displacement risk assessments, which
743 regional authorities could incorporate in urban development plans, zoning regulations or
744 required building codes (IDMC, 2019). Mozambique, like many countries, is exposed not only
745 to TCs but also other climate-related hazards, such as droughts, and at the same time facing
746 socio-economic challenges, making it all the more important to understand and anticipate risks
747 in a changing climate. Our approach may hence be extended to large-n impact attribution,
748 using, for example, global counterfactual climate datasets (Mengel et al., 2021).

Code availability

750 The source code for this study is available from
751 https://github.com/BenediktMester/TC_Idai_attribution.
752

Data availability

754 Satellite imagery is used with the permission of Atmospheric and Environmental Research &
755 African Risk Capacity. Output of the flood depth algorithm, GeoClaw results, and TC Idai wind
756 speed files can be accessed at https://zenodo.org/record/6907855 (Mester et al., 2022). GHS
757 gridded population data is available at https://data.jrc.ec.europa.eu/dataset/jrc-ghsl-
758 ghs_pop_gpw4_globe_r2015a#dataaccess.
759 National borders of Mozambique were obtained from https://gadm.org/data.html. For the
760 trendline analysis of annual means of maximum wind speeds we use IBTrACS Version 4
761 database, accessible at https://www.ncei.noaa.gov/data/international-best-track-archive-for-
762 climate-stewardship-ibtracs/v04r00/access/netcdf/IBTrACS.ALL.v04r00.nc.
763

764 All data used for the figures are publicly available. Maps were generated with QGIS, which
765 can be downloaded at https://www.qgis.org/. Satellite imagery background by © Google Maps
766 can be accessed via http://mt0.google.com/vt/lyrs=s&hl=en&x={x}&y={y}&z={z}. We used
767 IBTrACS Version 4 to extract the trajectory data of tropical cyclone Idai, availabe at
768 https://www.ncei.noaa.gov/products/international-best-track-archive?name=ib-v4-access.
769 Mozambique admin level 4 shapefiles for Beira are available at
770 https://data.humdata.org/dataset/mozambique-admin-level-4-beira-and-dondo-
771 neighbourhood-boundaries. GSHHG shoreline data can be accessed via
772 https://www.ngdc.noaa.gov/mgg/shorelines/data/gshhg/latest/.

Author contributions

774 B.M. and J.S. designed the study, with contributions from T.V., C.O., and K.F. T.V. designed
775 and performed coastal flood model calculations. S.B. estimated flood depths from satellite
776 imagery. B.M. computed the number of affected people and displacements. B.M. and J.S.

777 analyzed the results, and C.O. and K.F. contributed to the interpretation. B.M. and J.S. jointly
778 wrote the paper, with contributions from T.V., S.B., and C.O.

Competing interests

780 The authors declare no competing interests.

Acknowledgments

789

References

791

792 Angélil, O., Perkins-Kirkpatrick, S., Alexander, L.V., Stone, D., Donat, M.G., Wehner, M.,
793   Shiogama, H., Ciavarella, A., Christidis, N., 2016. Comparing regional precipitation
794   and temperature extremes in climate model and reanalysis products. Weather Clim.
795   Extrem. 13, 35–43. https://doi.org/10.1016/j.wace.2016.07.001
796 Archila Bustos, M.F., Hall, O., Niedomysl, T., Ernstson, U., 2020. A pixel level evaluation of
797   five multitemporal global gridded population datasets: a case study in Sweden,
798   1990–2015. Popul. Environ. 42, 255–277. https://doi.org/10.1007/s11111-020-00360-
799   8
800 Atmospheric and Environmental Research & African Risk Capacity, 2022. Flood depictions:
801   AER AFED v05r01.
802 Beal, L.M., Vialard, J., Roxy, M.K., lead authors, 2019. IndOOS-2: A roadmap to sustained
803   observations of the Indian Ocean for 2020-203 CLIVAR-4/2019, GOOS-237, 206 pp.,
804   218.
805 Bergensia, 2019. Red Cross: 90 Percent of Beira in Mozambique Destroyed by Cyclone Idai.
806   URL: https://bergensia.com/red-cross-90-percent-of-beira-in-mozambique-destroyed-
807   by-cyclone-idai/.
808 Bernhofen, M.V., Whyman, C., Trigg, M.A., Sleigh, P.A., Smith, A.M., Sampson, C.C.,
809   Yamazaki, D., Ward, P.J., Rudari, R., Pappenberger, F., Dottori, F., Salamon, P.,
810   Winsemius, H.C., 2018. A first collective validation of global fluvial flood models for
811   major floods in Nigeria and Mozambique. Environ. Res. Lett. 13, 104007.
812   https://doi.org/10.1088/1748-9326/aae014
813 Bilskie, M.V., Hagen, S.C., 2018. Defining Flood Zone Transitions in Low-Gradient Coastal
814   Regions. Geophys. Res. Lett. 45, 2761–2770. https://doi.org/10.1002/2018GL077524
815 Bloemendaal, N., de Moel, H., Martinez, A.B., Muis, S., Haigh, I.D., van der Wiel, K.,
816   Haarsma, R.J., Ward, P.J., Roberts, M.J., Dullaart, J.C.M., Aerts, J.C.J.H., 2022. A
817   globally consistent local-scale assessment of future tropical cyclone risk. Sci. Adv. 8,
818   eabm8438. https://doi.org/10.1126/sciadv.abm8438

819   Bloemendaal, N., Haigh, I.D., de Moel, H., Muis, S., Haarsma, R.J., Aerts, J.C.J.H., 2020.
820   Generation of a global synthetic tropical cyclone hazard dataset using STORM. Sci.
821   Data 7, 40. https://doi.org/10.1038/s41597-020-0381-2

822   Bloemendaal, N., Moel, H. de, Mol, J.M., Bosma, P.R.M., Polen, A.N., Collins, J.M., 2021.
823   Adequately reflecting the severity of tropical cyclones using the new Tropical Cyclone
824   Severity Scale. Environ. Res. Lett. 16, 014048. https://doi.org/10.1088/1748-
825   9326/abd131

826   Blöschl, G., Hall, J., Viglione, A., Perdigão, R.A.P., Parajka, J., Merz, B., Lun, D., Arheimer,
827   B., Aronica, G.T., Bilibashi, A., Boháč, M., Bonacci, O., Borga, M., Čanjevac, I.,
828   Castellarin, A., Chirico, G.B., Claps, P., Frolova, N., Ganora, D., Gorbachova, L., Gül,
829   A., Hannaford, J., Harrigan, S., Kireeva, M., Kiss, A., Kjeldsen, T.R., Kohnová, S.,
830   Koskela, J.J., Ledvinka, O., Macdonald, N., Mavrova-Guirguinova, M., Mediero, L.,
831   Merz, R., Molnar, P., Montanari, A., Murphy, C., Osuch, M., Ovcharuk, V., Radevski,
832   I., Salinas, J.L., Sauquet, E., Šraj, M., Szolgay, J., Volpi, E., Wilson, D., Zaimi, K.,
833   Živković, N., 2019. Changing climate both increases and decreases European river
834   floods. Nature 573, 108–111. https://doi.org/10.1038/s41586-019-1495-6

835   Bryant, S., McGrath, H., Boudreault, M., 2022. Gridded flood depth estimates from satellite-
836   derived inundations. Nat. Hazards Earth Syst. Sci. 22, 1437–1450.
837   https://doi.org/10.5194/nhess-22-1437-2022

838   Cattaneo, C., Beine, M., Fröhlich, C.J., Kniveton, D., Martinez-Zarzoso, I., Mastrorillo, M.,
839   Millock, K., Piguet, E., Schraven, B., 2019. Human Migration in the Era of Climate
840   Change. Rev. Environ. Econ. Policy 13, 189–206.
841   https://doi.org/10.1093/reep/rez008

842   Chavas, D.R., Lin, N., Dong, W., Lin, Y., 2016. Observed Tropical Cyclone Size Revisited. J.
843   Clim. 29, 2923–2939. https://doi.org/10.1175/JCLI-D-15-0731.1

844   Church, J.A., Clark, P.U., Cazenave, A., Gregory, J.M., Jevrejeva, S., Levermann, A.,
845   Merrifield, M.A., Milne, G.A., Nerem, R.S., Nunn, P.D., Payne, A.J., Pfeffer, W.T.,
846   Stammer, D., Unnikrishnan, A.S., 2013. Sea Level Change. In: Climate Change
847   2013: The Physical Science Basis. Contribution of Working Group I to the Fifth
848   Assessment Report of the Intergovernmental Panel on Climate Change [Stocker,
849   T.F., D. Qin, G.-K. Plattner, M. Tignor, S.K. Allen, J. Boschung, A. Nauels, Y. Xia, V.
850   Bex and P.M. Midgley (eds.)]. Cambridge University Press, Cambridge, United
851   Kingdom and New York, NY, USA, pp. 1137–1216.

852   Church, J.A., White, N.J., 2011. Sea-Level Rise from the Late 19th to the Early 21st Century.
853   Surv. Geophys. 32, 585–602. https://doi.org/10.1007/s10712-011-9119-1

854   Church, J.A., White, N.J., Coleman, R., Lambeck, K., Mitrovica, J.X., 2004. Estimates of the
855   Regional Distribution of Sea Level Rise over the 1950–2000 Period. J. Clim. 17,
856   2609–2625. https://doi.org/10.1175/1520-0442(2004)017<2609:EOTRDO>2.0.CO;2

857   Cissé, G., McLeman, R., Adams, H., Aldunce, P., Bowen, K., Campbell-Lendrum, D.,
858   Clayton, S., Ebi, K.L., Hess, J., Huang, C., Liu, Q., McGregor, G., Semenza, J.,
859   Tirado, M.C., 2022. Health, Wellbeing, and the Changing Structure of Communities.
860   In: Climate Change 2022: Impacts, Adaptation, and Vulnerability. Contribution of
861   Working Group II to the Sixth Assessment Report of the Intergovernmental Panel on
862   Climate Change [H.-O. Pörtner, D.C. Roberts, M. Tignor, E.S. Poloczanska, K.
863   Mintenbeck, A. Alegría, M. Craig, S. Langsdorf, S. Löschke, V. Möller, A. Okem, B.
864   Rama (eds.)]. Cambridge University Press, Cambridge, UK and New York, NY, USA,
865   pp. 1041-1170, doi:10.1017/9781009325844.009.

866   CMEMS, 2021. Global ocean gridded L4 sea surface heights and derived variables
867   reprocessed (1993-ongoing). E.U. Copernicus Marine Service (CMEMS).
868   Downloaded 2021-08-02.

869   Cohen, S., Brakenridge, G.R., Kettner, A., Bates, B., Nelson, J., McDonald, R., Huang, Y.-F.,
870   Munasinghe, D., Zhang, J., 2018. Estimating Floodwater Depths from Flood
871   Inundation Maps and Topography. JAWRA J. Am. Water Resour. Assoc. 54, 847–
872   858. https://doi.org/10.1111/1752-1688.12609

873   Custer, R., Nishijima, K., 2015. Flood vulnerability assessment of residential buildings by

874   explicit damage process modelling. Nat. Hazards 78, 461–496.
875   https://doi.org/10.1007/s11069-015-1725-7

876 Dangendorf Sönke, Marcos Marta, Wöppelmann Guy, Conrad Clinton P., Frederikse
877   Thomas, Riva Riccardo, 2017. Reassessment of 20th century global mean sea level
878   rise. Proc. Natl. Acad. Sci. 114, 5946–5951.
879   https://doi.org/10.1073/pnas.1616007114

880 Desai, B., Bresch, D.N., Cazabat, C., Hochrainer-Stigler, S., Mechler, R., Ponserre, S.,
881   Schewe, J., 2021. Addressing the human cost in a changing climate. Science 372,
882   1284–1287. https://doi.org/10.1126/science.abh4283

883 Dullaart, J.C.M., Muis, S., Bloemendaal, N., Chertova, M.V., Couasnon, A., Aerts, J.C.J.H.,
884   2021. Accounting for tropical cyclones more than doubles the global population
885   exposed to low-probability coastal flooding. Commun. Earth Environ. 2, 135.
886   https://doi.org/10.1038/s43247-021-00204-9

887 Eilander, D., Couasnon, A., Leijnse, T., Ikeuchi, H., Yamazaki, D., Muis, S., Dullaart, J.,
888   Winsemius, H.C., Ward, P.J., 2022. A globally-applicable framework for compound
889   flood hazard modeling. EGUsphere 2022, 1–40. https://doi.org/10.5194/egusphere-
890   2022-149

891 Emanuel, K., 2005. Increasing destructiveness of tropical cyclones over the past 30 years.
892   Nature 436, 686–688. https://doi.org/10.1038/nature03906

893 Emanuel, K., Ravela, S., Vivant, E., Risi, C., 2006. A Statistical Deterministic Approach to
894   Hurricane Risk Assessment. Bull. Am. Meteorol. Soc. 87, 299–314.
895   https://doi.org/10.1175/BAMS-87-3-299

896 Emanuel, K.A., 2013. Downscaling CMIP5 climate models shows increased tropical cyclone
897   activity over the 21st century. Proc. Natl. Acad. Sci. U. S. A. 110, 12219–12224.
898   https://doi.org/10.1073/pnas.1301293110

899 Emanuel, K.A., 1987. The dependence of hurricane intensity on climate. Nature 326, 483–
900   485. https://doi.org/10.1038/326483a0

901 Emerton, R., Cloke, H., Ficchi, A., Hawker, L., de Wit, S., Speight, L., Prudhomme, C.,
902   Rundell, P., West, R., Neal, J., Cuna, J., Harrigan, S., Titley, H., Magnusson, L.,
903   Pappenberger, F., Klingaman, N., Stephens, E., 2020. Emergency flood bulletins for
904   Cyclones Idai and Kenneth: A critical evaluation of the use of global flood forecasts
905   for international humanitarian preparedness and response. Int. J. Disaster Risk
906   Reduct. 50, 101811. https://doi.org/10.1016/j.ijdrr.2020.101811

907 Fowler, H.J., Lenderink, G., Prein, A.F., Westra, S., Allan, R.P., Ban, N., Barbero, R., Berg,
908   P., Blenkinsop, S., Do, H.X., Guerreiro, S., Haerter, J.O., Kendon, E.J., Lewis, E.,
909   Schaer, C., Sharma, A., Villarini, G., Wasko, C., Zhang, X., 2021. Anthropogenic
910   intensification of short-duration rainfall extremes. Nat. Rev. Earth Environ. 2, 107–
911   122. https://doi.org/10.1038/s43017-020-00128-6

912 Fox-Kemper, B., Hewitt, H.T., Xiao, C., Aðalgeirsdóttir, G., Drijfhout, S.S., Edwards, T.L.,
913   Golledge, N.R., Hemer, M., Kopp, R.E., Krinner, G., Mix, A., Notz, D., Nowicki, S.,
914   Nurhati, I.S., Ruiz, L., Sallée, J.-B., Slangen, A.B.A., Yu, Y., 2021. Ocean,
915   Cryosphere and Sea Level Change. In Climate Change 2021: The Physical Science
916   Basis. Contribution of Working Group I to the Sixth Assessment Report of the
917   Intergovernmental Panel on Climate Change [Masson-Delmotte, V., P. Zhai, A.
918   Pirani, S.L. Connors, C. Péan, S. Berger, N. Caud, Y. Chen, L. Goldfarb, M.I. Gomis,
919   M. Huang, K. Leitzell, E. Lonnoy, J.B.R. Matthews, T.K. Maycock, T. Waterfield, O.
920   Yelekçi, R. Yu, and B. Zhou (eds.)]. Cambridge University Press, Cambridge, United
921   Kingdom and New York, NY, USA, pp. 1211–1362.

922 Frame, D.J., Rosier, S.M., Noy, I., Harrington, L.J., Carey-Smith, T., Sparrow, S.N., Stone,
923   D.A., Dean, S.M., 2020a. Climate change attribution and the economic costs of
924   extreme weather events: a study on damages from extreme rainfall and drought.
925   Clim. Change 162, 781–797. https://doi.org/10.1007/s10584-020-02729-y

926 Frame, D.J., Wehner, M.F., Noy, I., Rosier, S.M., 2020b. The economic costs of Hurricane
927   Harvey attributable to climate change. Clim. Change 160, 271–281.
928   https://doi.org/10.1007/s10584-020-02692-8

Freire, S., MacManus, K., Pesaresi, M., Doxsey-Whitfield, E., Mills, J., 2016. Development of new open and free multi-temporal global population grids at 250m resolution. Paper presented at the 19th AGILE Conference on Geographic Information Science, Helsinki, Finland.

GADM, 2018. Database of Global Administrative Areas.

Galantowicz, J.F., Picton, J., 2021. Flood Mapping with Passive Microwave Remote Sensing: Current Capabilities and Directions for Future Development, in: Earth Observation for Flood Applications. Elsevier, p. 28.

Garner Andra J., Mann Michael E., Emanuel Kerry A., Kopp Robert E., Lin Ning, Alley Richard B., Horton Benjamin P., DeConto Robert M., Donnelly Jeffrey P., Pollard David, 2017. Impact of climate change on New York City's coastal flood hazard: Increasing flood heights from the preindustrial to 2300 CE. Proc. Natl. Acad. Sci. 114, 11861–11866. https://doi.org/10.1073/pnas.1703568114

Geiger, T., Frieler, K., Bresch, D.N., 2018. A global historical data set of tropical cyclone exposure (TCE-DAT). Earth Syst. Sci. Data 10, 185–194. https://doi.org/10.5194/essd-10-185-2018

Gemenne, F., 2011. Why the numbers don't add up: A review of estimates and predictions of people displaced by environmental changes. Glob. Environ. Change, Migration and Global Environmental Change – Review of Drivers of Migration 21, S41–S49. https://doi.org/10.1016/j.gloenvcha.2011.09.005

Google Maps (a), 2022. Mozambique. Satellite image. URL: http://mt0.google.com/vt/lyrs=s&hl=en&x={x}&y={y}&z={z}. Accessed on 2022-04-27.

Google Maps (b), 2022. Greater Area of Beira, Mozambique. Satellite image. URL: http://mt0.google.com/vt/lyrs=s&hl=en&x={x}&y={y}&z={z}. Accessed on 2022-04-27.

Gudmundsson, L., Boulange, J., Do, H.X., Gosling, S.N., Grillakis, M.G., Koutroulis, A.G., Leonard, M., Liu, J., Müller Schmied, H., Papadimitriou, L., Pokhrel, Y., Seneviratne, S.I., Satoh, Y., Thiery, W., Westra, S., Zhang, X., Zhao, F., 2021. Globally observed trends in mean and extreme river flow attributed to climate change. Science 371, 1159–1162. https://doi.org/10.1126/science.aba3996

Guerreiro, S.B., Fowler, H.J., Barbero, R., Westra, S., Lenderink, G., Blenkinsop, S., Lewis, E., Li, X.-F., 2018. Detection of continental-scale intensification of hourly rainfall extremes. Nat. Clim. Change 8, 803–807. https://doi.org/10.1038/s41558-018-0245-3

Guha-Sapir, D., Below, R., Hoyois, P., 2022. EM-DAT: The CRED/OFDA International Disaster Database. Université Catholique de Louvain-Brussels, Belgium.

Gulev, S.K., Thorne, P.W., Ahn, J., Dentener, F.J., Domingues, C.M., Gerland, S., Gong, D., Kaufman, D.S., Nnamchi, H.C., Quaas, J., Rivera, J.A., Sathyendranath, S., Smith, S.L., Trewin, B., von Schuckmann, K., Vose, R.S., 2021. Changing State of the Climate System. In Climate Change 2021: The Physical Science Basis. Contribution of Working Group I to the Sixth Assessment Report of the Intergovernmental Panel on Climate Change [Masson-Delmotte, V., P. Zhai, A. Pirani, S.L. Connors, C. Péan, S. Berger, N. Caud, Y. Chen, L. Goldfarb, M.I. Gomis, M. Huang, K. Leitzell, E. Lonnoy, J.B.R. Matthews, T.K. Maycock, T. Waterfield, O. Yelekçi, R. Yu, and B. Zhou (eds.)]. Cambridge University Press. In Press.

Han, W., Meehl, G.A., Rajagopalan, B., Fasullo, J.T., Hu, A., Lin, J., Large, W.G., Wang, J., Quan, X.-W., Trenary, L.L., Wallcraft, A., Shinoda, T., Yeager, S., 2010. Patterns of Indian Ocean sea-level change in a warming climate. Nat. Geosci. 3, 546–550. https://doi.org/10.1038/ngeo901

HDX, 2019. Mozambique admin level 4 - Beira and Dondo neighbourhood boundaries.

Holland, G.J., 1980. An Analytic Model of the Wind and Pressure Profiles in Hurricanes. Mon. Weather Rev. 108, 1212–1218. https://doi.org/10.1175/1520-0493(1980)108<1212:AAMOTW>2.0.CO;2

Hollinger, M., Sienkevych, O., 2019. The role of local and regional governments in protecting internally displaced persons (IDPs).

IDMC, 2022. "IDMC Global Report on Internal Displacement 2022 Displacement Dataset." https://www.internal-displacement.org/database/displacement-data.

IDMC, 2019. Unveiling the cost of internal displacement, The ripple effect: economic impacts of internal displacement.

Irish, J.L., Sleath, A., Cialone, M.A., Knutson, T.R., Jensen, R.E., 2014. Simulations of Hurricane Katrina (2005) under sea level and climate conditions for 1900. Clim. Change 122, 635–649. https://doi.org/10.1007/s10584-013-1011-1

Kam, P.M., Aznar-Siguan, G., Schewe, J., Milano, L., Ginnetti, J., Willner, S., McCaughey, J.W., Bresch, D.N., 2021. Global warming and population change both heighten future risk of human displacement due to river floods. Environ. Res. Lett. 16, 044026. https://doi.org/10.1088/1748-9326/abd26c

Knapp, K.R., Kruk, M.C., Levinson, D.H., Diamond, H.J., Neumann, C.J., 2010. The International Best Track Archive for Climate Stewardship (IBTrACS): Unifying Tropical Cyclone Data. Bulletin of the American Meteorological Society 91 (3): 363-76.

Knutson, T., Camargo, S.J., Chan, J.C.L., Emanuel, K., Ho, C.-H., Kossin, J., Mohapatra, M., Satoh, M., Sugi, M., Walsh, K., Wu, L., 2020. Tropical Cyclones and Climate Change Assessment: Part II: Projected Response to Anthropogenic Warming. Bull. Am. Meteorol. Soc. 101, E303–E322. https://doi.org/10.1175/BAMS-D-18-0194.1

Knutson, T., Camargo, S.J., Chan, J.C.L., Emanuel, K., Ho, C.-H., Kossin, J., Mohapatra, M., Satoh, M., Sugi, M., Walsh, K., Wu, L., 2019. Tropical Cyclones and Climate Change Assessment: Part I: Detection and Attribution. Bull. Am. Meteorol. Soc. 100, 1987–2007. https://doi.org/10.1175/BAMS-D-18-0189.1

Knutson, T.R., Sirutis, J.J., Zhao, M., Tuleya, R.E., Bender, M., Vecchi, G.A., Villarini, G., Chavas, D., 2015. Global Projections of Intense Tropical Cyclone Activity for the Late Twenty-First Century from Dynamical Downscaling of CMIP5/RCP4.5 Scenarios. J. Clim. 28, 7203–7224. https://doi.org/10.1175/JCLI-D-15-0129.1

Kossin, J.P., Knapp, K.R., Vimont, D.J., Murnane, R.J., Harper, B.A., 2007. A globally consistent reanalysis of hurricane variability and trends. Geophys. Res. Lett. 34. https://doi.org/10.1029/2006GL028836

Kossin, J.P., Olander, T.L., Knapp, K.R., 2013. Trend Analysis with a New Global Record of Tropical Cyclone Intensity. J. Clim. 26, 9960–9976. https://doi.org/10.1175/JCLI-D-13-00262.1

Kulp, S.A., Strauss, B.H., 2021. CoastalDEM v2.1: A high-accuracy and high-resolution global coastal elevation model trained on ICESat-2 satellite lidar. Climate Central Scientific Report 17.

Kulp, S.A., Strauss, B.H., 2018. CoastalDEM: A global coastal digital elevation model improved from SRTM using a neural network. Remote Sens. Environ. 206, 231–239. https://doi.org/10.1016/j.rse.2017.12.026

Lee, J.-Y., Marotzke, J., Bala, G., Cao, L., Corti, S., Dunne, J.P., Engelbrecht, F., Fischer, E., Fyfe, J.C., Jones, C., Maycock, A., Mutemi, J., Ndiaye, O., Panickal, S., Zhou, T., 2021. Future Global Climate: Scenario-Based Projections and Near-Term Information. In Climate Change 2021: The Physical Science Basis. Contribution of Working Group I to the Sixth Assessment Report of the Intergovernmental Panel on Climate Change [Masson-Delmotte, V., P. Zhai, A. Pirani, S.L. Connors, C. Péan, S. Berger, N. Caud, Y. Chen, L. Goldfarb, M.I. Gomis, M. Huang, K. Leitzell, E. Lonnoy, J.B.R. Matthews, T.K. Maycock, T. Waterfield, O. Yelekçi, R. Yu, and B. Zhou (eds.)]. C. Cambridge University Press, Cambridge, United Kingdom and New York, NY, USA, pp. 553–672.

Leyk, S., Gaughan, A.E., Adamo, S.B., de Sherbinin, A., Balk, D., Freire, S., Rose, A., Stevens, F.R., Blankespoor, B., Frye, C., Comenetz, J., Sorichetta, A., MacManus, K., Pistolesi, L., Levy, M., Tatem, A.J., Pesaresi, M., 2019. The spatial allocation of population: a review of large-scale gridded population data products and their fitness for use. Earth Syst. Sci. Data 11, 1385–1409. https://doi.org/10.5194/essd-11-1385-2019

Lin, N., Emanuel, K., Oppenheimer, M., Vanmarcke, E., 2012. Physically based assessment of hurricane surge threat under climate change. Nat. Clim. Change 2, 462–467.

https://doi.org/10.1038/nclimate1389

Lin, N., Lane, P., Emanuel, K.A., Sullivan, R.M., Donnelly, J.P., 2014. Heightened hurricane surge risk in northwest Florida revealed from climatological-hydrodynamic modeling and paleorecord reconstruction. J. Geophys. Res. Atmospheres 119, 8606–8623. https://doi.org/10.1002/2014JD021584

Lindsay, J.B., 2014. The Whitebox Geospatial Analysis Tools Project and Open-Access GIS. Proc. GIS Res. UK 22nd Annu. Conf. Univ. Glasg. 16–18.

Luu, L.N., Scussolini, P., Kew, S., Philip, S., Hariadi, M.H., Vautard, R., Van Mai, K., Van Vu, T., Truong, K.B., Otto, F., van der Schrier, G., van Aalst, M.K., van Oldenborgh, G.J., 2021. Attribution of typhoon-induced torrential precipitation in Central Vietnam, October 2020. Clim. Change 169, 24. https://doi.org/10.1007/s10584-021-03261-3

Lyard, F.H., Allain, D.J., Cancet, M., Carrère, L., Picot, N., 2021. FES2014 global ocean tide atlas: design and performance. Ocean Sci. 17, 615–649. https://doi.org/10.5194/os-17-615-2021

Mandli, K.T., Dawson, C.N., 2014. Adaptive mesh refinement for storm surge. Ocean Model. 75, 36–50. https://doi.org/10.1016/j.ocemod.2014.01.002

McAdam, J., 2022. Evacuations: a form of disaster displacement? Forced Migr. Rev. 56–57.

Mengel, M., Treu, S., Lange, S., Frieler, K., 2021. ATTRICI v1.1 – counterfactual climate for impact attribution. Geosci. Model Dev. 14, 5269–5284. https://doi.org/10.5194/gmd-14-5269-2021

Mester, B., Vogt, T., Bryant, S., Otto, C., Frieler, K., Schewe, J., 2022. TC Idai attribution study - data collection v1.1 (Version v1.1). doi: 10.5281/zenodo.6907855.

Mester, B., Willner, S.N., Frieler, K., Schewe, J., 2021. Evaluation of river flood extent simulated with multiple global hydrological models and climate forcings. Environ. Res. Lett. 16, 094010. https://doi.org/10.1088/1748-9326/ac188d

Muis, S., Apecechea, M.I., Dullaart, J., de Lima Rego, J., Madsen, K.S., Su, J., Yan, K., Verlaan, M., 2020. A High-Resolution Global Dataset of Extreme Sea Levels, Tides, and Storm Surges, Including Future Projections. Front. Mar. Sci. 7. https://doi.org/10.3389/fmars.2020.00263

Nicholls, R.J., Lincke, D., Hinkel, J., Brown, S., Vafeidis, A.T., Meyssignac, B., Hanson, S.E., Merkens, J.-L., Fang, J., 2021. A global analysis of subsidence, relative sea-level change and coastal flood exposure. Nat. Clim. Change 11, 338–342. https://doi.org/10.1038/s41558-021-00993-z

Nott, J., Hayne, M., 2001. High frequency of 'super-cyclones' along the Great Barrier Reef over the past 5,000 years. Nature 413, 508–512. https://doi.org/10.1038/35097055

OCHA, 2004. Guiding Principles on Internal Displacement.

Oldenborgh, G.J. van, Wiel, K. van der, Sebastian, A., Singh, R., Arrighi, J., Otto, F., Haustein, K., Li, S., Vecchi, G., Cullen, H., 2017. Attribution of extreme rainfall from Hurricane Harvey, August 2017. Environ. Res. Lett. 12, 124009. https://doi.org/10.1088/1748-9326/aa9ef2

O'Neill, B., van Aalst, M., Zaiton Ibrahim, Z., Berrang Ford, L., Bhadwal, S., Buhaug, H., Diaz, D., Frieler, K., Garschagen, M., Magnan, A., Midgley, G., Mirzabaev, A., Thomas, A., Warren, R., 2022. Key Risks Across Sectors and Regions. In: Climate Change 2022: Impacts, Adaptation, and Vulnerability. Contribution of Working Group II to the Sixth Assessment Report of the Intergovernmental Panel on Climate Change [H.-O. Pörtner, D.C. Roberts, M. Tignor, E.S. Poloczanska, K. Mintenbeck, A. Alegría, M. Craig, S. Langsdorf, S. Löschke, V. Möller, A. Okem, B. Rama (eds.)]. Cambridge University Press.

Otto, F.E.L., Harrington, L., Schmitt, K., Philip, S., Kew, S., Oldenborgh, G.J. van, Singh, R., Kimutai, J., Wolski, P., 2020. Challenges to Understanding Extreme Weather Changes in Lower Income Countries. Bull. Am. Meteorol. Soc. 101, E1851–E1860. https://doi.org/10.1175/BAMS-D-19-0317.1

Patricola, C.M., Wehner, M.F., 2018. Anthropogenic influences on major tropical cyclone events. Nature 563, 339–346. https://doi.org/10.1038/s41586-018-0673-2

Pekel, J.-F., Cottam, A., Gorelick, N., Belward, A.S., 2016. High-resolution mapping of global

1094   surface water and its long-term changes. Nature 540, 418–422.
1095   https://doi.org/10.1038/nature20584
1096   Probst, P., Annunziato, A., 2019. Tropical Cyclone IDAI: analysis of the wind, rainfall and
1097   storm surge impact. Join Research Centre (EUROPEAN COMMISSION). URL:
1098   https://www.humanitarianresponse.info/sites/www.humanitarianresponse.info/files/do
1099   cuments/files/joint_research_centre_analysis_of_wind_rainfall_and_storm_surge_im
1100   pact_09_april_2019.pdf.
1101   ReliefWeb, 2019a. Mozambique: Cyclone Idai & Floods Flash Update No. 10, 26 March
1102   2019. URL: https://reliefweb.int/report/mozambique/mozambique-cyclone-idai-floods-
1103   flash-update-no-10-26-march-2019. Accessed on 2023-05-15.
1104   ReliefWeb, 2019b. 'The First City Completely Devastated by Climate Change' Tries to
1105   Rebuild after Cyclone Idai. URL: https://reliefweb.int/report/mozambique/first-city-
1106   completely-devastated-climate-change-tries-rebuild-after-cyclone-idai.
1107   Resio, D.T., Irish, J.L., 2016. Tropical Cyclone Storm Surge Risk, in: Handbook of Coastal
1108   and Ocean Engineering. WORLD SCIENTIFIC, pp. 1405–1422.
1109   https://doi.org/10.1142/9789813204027_0049
1110   Riahi, K., van Vuuren, D.P., Kriegler, E., Edmonds, J., O'Neill, B.C., Fujimori, S., Bauer, N.,
1111   Calvin, K., Dellink, R., Fricko, O., Lutz, W., Popp, A., Cuaresma, J.C., Kc, S.,
1112   Leimbach, M., Jiang, L., Kram, T., Rao, S., Emmerling, J., Ebi, K., Hasegawa, T.,
1113   Havlik, P., Humpenöder, F., Da Silva, L.A., Smith, S., Stehfest, E., Bosetti, V., Eom,
1114   J., Gernaat, D., Masui, T., Rogelj, J., Strefler, J., Drouet, L., Krey, V., Luderer, G.,
1115   Harmsen, M., Takahashi, K., Baumstark, L., Doelman, J.C., Kainuma, M., Klimont,
1116   Z., Marangoni, G., Lotze-Campen, H., Obersteiner, M., Tabeau, A., Tavoni, M., 2017.
1117   The Shared Socioeconomic Pathways and their energy, land use, and greenhouse
1118   gas emissions implications: An overview. Glob. Environ. Change 42, 153–168.
1119   https://doi.org/10.1016/j.gloenvcha.2016.05.009
1120   Sauer, I.J., Reese, R., Otto, C., Geiger, T., Willner, S.N., Guillod, B.P., Bresch, D.N., Frieler,
1121   K., 2021. Climate signals in river flood damages emerge under sound regional
1122   disaggregation. Nat. Commun. 12, 2128. https://doi.org/10.1038/s41467-021-22153-
1123   9
1124   Scherrer, S.C., Fischer, E.M., Posselt, R., Liniger, M.A., Croci-Maspoli, M., Knutti, R., 2016.
1125   Emerging trends in heavy precipitation and hot temperature extremes in Switzerland.
1126   J. Geophys. Res. Atmospheres 121, 2626–2637.
1127   https://doi.org/10.1002/2015JD024634
1128   Schiavina, M., Freire, S., MacManus, K., 2019. GHS population grid multitemporal (1975,
1129   1990, 2000, 2015) R2019A. European Commission, Joint Research Centre (JRC).
1130   https://doi.org/10.2905/42E8BE89-54FF-464E-BE7B-BF9E64DA5218
1131   Shen, X., Wang, D., Mao, K., Anagnostou, E., Hong, Y., 2019. Inundation Extent Mapping by
1132   Synthetic Aperture Radar: A Review. Remote Sens. 11, 879.
1133   https://doi.org/10.3390/rs11070879
1134   Shepherd, T.G., 2016. A Common Framework for Approaches to Extreme Event Attribution.
1135   Curr. Clim. Change Rep. 2, 28–38. https://doi.org/10.1007/s40641-016-0033-y
1136   Shepherd, T.G., Boyd, E., Calel, R.A., Chapman, S.C., Dessai, S., Dima-West, I.M., Fowler,
1137   H.J., James, R., Maraun, D., Martius, O., Senior, C.A., Sobel, A.H., Stainforth, D.A.,
1138   Tett, S.F.B., Trenberth, K.E., van den Hurk, B.J.J.M., Watkins, N.W., Wilby, R.L.,
1139   Zenghelis, D.A., 2018. Storylines: an alternative approach to representing uncertainty
1140   in physical aspects of climate change. Clim. Change 151, 555–571.
1141   https://doi.org/10.1007/s10584-018-2317-9
1142   Strauss, B.H., Orton, P.M., Bittermann, K., Buchanan, M.K., Gilford, D.M., Kopp, R.E., Kulp,
1143   S., Massey, C., Moel, H. de, Vinogradov, S., 2021. Economic damages from
1144   Hurricane Sandy attributable to sea level rise caused by anthropogenic climate
1145   change. Nat. Commun. 12, 2720. https://doi.org/10.1038/s41467-021-22838-1
1146   Takayabu, I., Hibino, K., Sasaki, H., Shiogama, H., Mori, N., Shibutani, Y., Takemi, T., 2015.
1147   Climate change effects on the worst-case storm surge: a case study of Typhoon
1148   Haiyan. Environ. Res. Lett. 10, 064011. https://doi.org/10.1088/1748-

9326/10/6/064011

The World Bank, 2022. World Development Indicators. Population, total - Mozambique.

Tozer, B., Sandwell, D.T., Smith, W.H.F., Olson, C., Beale, J.R., Wessel, P., 2019. Global Bathymetry and Topography at 15 Arc Sec: SRTM15+. Earth Space Sci. 6, 1847–1864. https://doi.org/10.1029/2019EA000658

Trenberth, K.E., Fasullo, J.T., Shepherd, T.G., 2015. Attribution of climate extreme events. Nat. Clim. Change 5, 725–730. https://doi.org/10.1038/nclimate2657

UK Government Office for Science, 2011. Foresight: Migration and Global Environmental Change (2011). Final Project Report [WWW Document]. GOV.UK. URL https://www.gov.uk/government/publications/migration-and-global-environmental-change-future-challenges-and-opportunities (accessed 1.4.23).

van Berchum, E.C., van Ledden, M., Timmermans, J.S., Kwakkel, J.H., Jonkman, S.N., 2020. Rapid flood risk screening model for compound flood events in Beira, Mozambique. Nat. Hazards Earth Syst. Sci. 20, 2633–2646. https://doi.org/10.5194/nhess-20-2633-2020

van den Hurk, B.J.J.M., Baldissera Pacchetti, M., Boere, E., Ciullo, A., Coulter, L., Dessai, S., Ercin, E., Goulart, H., Hamed, R., Hochrainer-Stigler, S., Koks, E., Kubiczek, P., Levermann, A., Mechler, R., van Meersbergen, M., Mester, B., Middelanis, R., Minderhoud, K., Mysiak, J., Nirandjan, S., van den Oord, G., Otto, C., Sayers, P., Schewe, J., Shepherd, T.G., Sillmann, J., Stuparu, D., Vogt, T., Witpas, K., 2023. Climate impact storylines for assessing socio-economic responses to remote events. Clim. Risk Manag. 100500. https://doi.org/10.1016/j.crm.2023.100500

van Oldenborgh, G.J., van der Wiel, K., Kew, S., Philip, S., Otto, F., Vautard, R., King, A., Lott, F., Arrighi, J., Singh, R., van Aalst, M., 2021. Pathways and pitfalls in extreme event attribution. Clim. Change 166, 13. https://doi.org/10.1007/s10584-021-03071-7

Warren, M., 2019. Why Cyclone Idai is one of the Southern Hemisphere's most devastating storms. Nature. https://doi.org/10.1038/d41586-019-00981-6

Webster, P.J., Holland, G.J., Curry, J.A., Chang, H.-R., 2005. Changes in Tropical Cyclone Number, Duration, and Intensity in a Warming Environment. Science 309, 1844–1846. https://doi.org/10.1126/science.1116448

Wessel, P., Smith, W., 1996. A global, self-consistent, hierarchical, high-resolution shoreline database. J. Geophys. Res. 101, 8741–8743. https://doi.org/10.1029/96JB00104

Wulder, M.A., White, J.C., Loveland, T.R., Woodcock, C.E., Belward, A.S., Cohen, W.B., Fosnight, E.A., Shaw, J., Masek, J.G., Roy, D.P., 2016. The global Landsat archive: Status, consolidation, and direction. Remote Sens. Environ. 185, 271–283.

Yamazaki, D., Ikeshima, D., Sosa, J., Bates, P.D., Allen, G.H., Pavelsky, T.M., 2019. MERIT Hydro: A High-Resolution Global Hydrography Map Based on Latest Topography Dataset. Water Resour. Res. 55, 5053–5073. https://doi.org/10.1029/2019WR024873

Zscheischler, J., Martius, O., Westra, S., Bevacqua, E., Raymond, C., Horton, R.M., van den Hurk, B., AghaKouchak, A., Jézéquel, A., Mahecha, M.D., Maraun, D., Ramos, A.M., Ridder, N.N., Thiery, W., Vignotto, E., 2020. A typology of compound weather and climate events. Nat. Rev. Earth Environ. 1, 333–347. https://doi.org/10.1038/s43017-020-0060-z